DEVELOPMENT OF A SIMPLIFIED FUEL OXIDATION MODEL FOR DEFECTIVE NUCLEAR FUEL

K. Shaheen and B.J. Lewis
Department of Chemistry and Chemical Engineering, Royal Military College of Canada, PO Box 17000, Kingston, Ontario, Canada, K7K 7B4
Corresponding Author: shaheen-k@rmc.ca

Abstract
The rare occurrence of sheath defects may lead to contact between the fuel and coolant, which may lead to fuel hyperstoichiometry, thus degrading fuel thermal performance and raising the potential for centreline melting. By simplifying a published mechanistic model, a treatment has been developed to predict fuel hyperstoichiometry using a one-dimensional oxygen transport equation coupled to a two-dimensional temperature equation, improving numerical robustness for possible implementation into fuel performance codes. The model has been validated against experimental measurements from commercial defective elements for normal operation, and has been used to predict the response of defective fuel under accident conditions.

1 Introduction
In rare cases (less than 0.1 % in CANDU reactors), defects can develop in the fuel sheath, possibly for one of the following reasons[1]: fretting, delayed hydrogen cracking, stress corrosion cracking, or fuel fabrication flaws. The degraded thermal performance of defective fuel increases the possibility of fuel centreline melting, which the CNSC (Canadian Nuclear Safety Commission) prohibits in safety analyses to guarantee pressure tube integrity[2]. Thus, there is a need to better understand defective fuel behaviour.

2 Review of Past Work
Upon entering the element through a sheath defect, the heavy water coolant flashes to D_2O gas, which oxidizes and deuterides the sheath. The gas also diffuses into the radial fuel cracks, oxidizing the fuel and releasing D_2 gas. The fuel oxidation reaction, the solid-state diffusion of oxygen in the fuel matrix, and the gaseous diffusion of the D_2/D_2O mixture in the fuel cracks and fuel-to-sheath gap are all temperature-dependent phenomena, where the temperature is itself oxidation-dependent through the fuel thermophysical properties.

In 2006, Ramirez et. al.[3] published a one-dimensional model for the radial transport of oxygen coupled to a heat balance equation. While this model does account for heat generation due to fission, stoichiometry dependence of thermophysical properties, and both Fickian and thermal diffusion of oxygen, it does not specifically include gas-phase transport of D_2/D_2O in the fuel cracks and fuel-to-sheath gap or oxidation/reduction kinetics. The Ramirez treatment also does not account for the axial diffusion of heat and mass, nor for the effects of plastic healing of fuel cracks.

In the same year, Higgs[4] published a more sophisticated two-dimensional (assuming azimuthal symmetry) mechanistic treatment addressing the key primary phenomena taking place in defective fuel. The model consists of a system of four coupled time-

dependent partial differential equations (PDEs) simulating axial gas-phase transport in the fuel-to-sheath gap, radial gas-phase transport in the fuel cracks, oxygen generation and two-dimensional interstitial transport in the fuel matrix, and heat generation and two-dimensional conduction in the solid fuel. The model accounts for the effects of sheath oxidation and deuteriding on the D_2/D_2O ratio in the fuel element, the effects of both Fickian and thermal diffusion of oxygen, the stoichiometry dependence of the fuel thermophysical properties, and the effects of crack healing in a plastic core on gas-phase transport and fuel oxidation.

The model of Higgs represents a complete conceptual accounting for the primary phenomena of defective fuel, and has been validated against experimental coulometric titration measurements performed on commercial defective elements at the Atomic Energy of Canada Limited – Chalk River Laboratories. However, the mechanistic model is also numerically intensive and thus relatively difficult to implement into Industry-Standard Toolsets currently used for fuel performance analysis. In addition, the treatment of the effects of plastic healing can cause occasional numerical instability in simulations of high-power elements. Thus, the goal of the current work is to produce a simplified treatment for fuel oxidation, where underlying phenomena are still captured using empirical correlations for increased robustness and numerical stability.

3 Model Development

3.1 Thermodynamics and Transport Phenomena

The uranium-oxygen phase diagram is shown in Figure 1 below[5]. At any given temperature, the equilibrium stoichiometry deviation x_e is the extent of stoichiometry deviation at which the oxygen partial pressures in the fuel and in the surrounding atmosphere are equal.

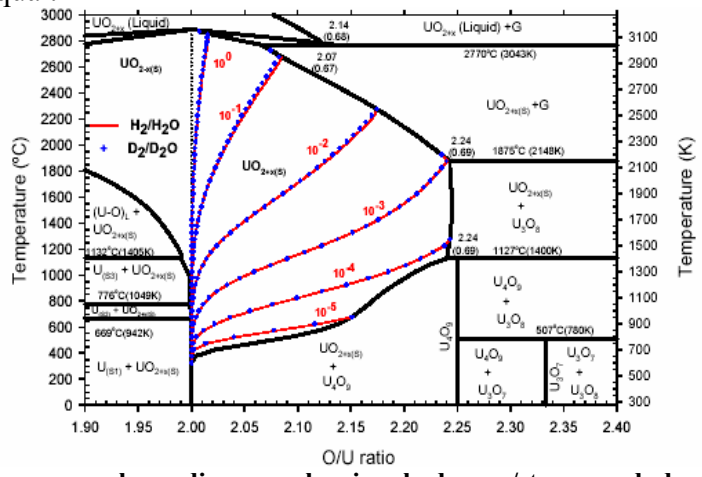

Figure 1 Uranium-oxygen phase diagram showing hydrogen/steam and deuterium/heavy water vapour fractions in equilibrium with temperature and O/U ratio.

The equilibrium partial pressure is associated with the reaction:

$$2D_2O(g) \Leftrightarrow O_2(g) + 2D_2(g) \qquad \textbf{Equation 1}$$

for which the equilibrium constant is:

$$K = \frac{p_{D_2}^2 p_{O_2}}{p_{D_2O}^2} \qquad \textbf{Equation 2}$$

Accordingly, x_e is related to the D_2/D_2O ratio. Since there is negligible difference in expressing the equilibrium with respect to the D_2/D_2O or H_2/H_2O ratio[5], an expression for x_e is developed as a function of the H_2/H_2O ratio (i.e., q/(1-q), where q is the hydrogen mole fraction), as shown in Ref. 5 and adopted in the current treatment.

Based on the observed results of mechanistic model simulations, the maximum stoichiometry deviation is associated with the generation of oxygen under the defect site, where the H_2/H_2O ratio in the fuel-to-sheath gap is lowest. While some oxidation may occur away from the defect site, the relative increase in the H_2/H_2O ratio in these regions would suppress the reaction. The axial stoichiometry deviation profile in the fuel element can be attributed to solid-state transport of oxygen from the primary oxidation site as a result of the oxygen concentration gradient. The simplified model can thus be conceptualized as shown in Figure 2 below:

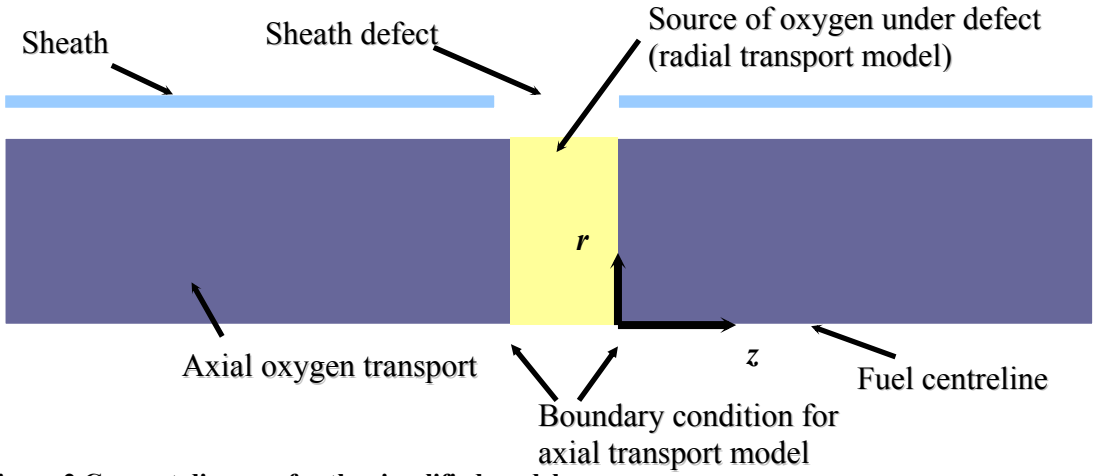

Figure 2 Concept diagram for the simplified model.

The one-dimensional oxygen transport equation under the defect site can be considered:

$$\frac{\partial x}{\partial t} = \frac{1}{r}\frac{\partial}{\partial r}\left[rD\left(\frac{\partial x}{\partial r} + x\frac{Q^*}{RT^2}\frac{\partial T}{\partial r} \right) \right] + \sigma_{fuel} R_{fuel}^{react} \qquad \textbf{Equation 3}$$

where x is the stoichiometry deviation in the fuel, t (s) is time, r (m) is radial position, T (K) is the fuel temperature, and Q^*, R, σ_{fuel}, and R_{fuel}^{react} are defined in Table 1. The change in stoichiometry deviation with respect to axial separation from the defect site z_{sep} is represented by a first-order kinetic process:

$$\frac{dx}{dz_{sep}} = -\xi x \qquad \textbf{Equation 4}$$

where ξ is a relaxation length dependent on the fuel and defect conditions. Together, Equations 3 and 4 provide a two-dimensional representation of oxygen transport to describe the stoichiometry deviation in the oxidized UO_{2+x} fuel. A two-dimensional representation of heat conduction in the fuel to determine the temperature profile is:

$$c_u C_p \frac{\partial T}{\partial t} = \frac{\partial}{\partial z}\left(k\frac{\partial T}{\partial z} + \frac{1}{r}\frac{\partial}{\partial r}\left(rk\frac{\partial T}{\partial r} \right) + \frac{P_{lin}}{\pi a_p^2}\left[\frac{(\kappa a_p)}{2I_1(\kappa a_p)} \right] I_o(\kappa r) \right) \qquad \textbf{Equation 5}$$

The expressions and values for the parameters used in Equations 3 and 5 are defined in Table 1 and further detailed in Ref 6.

Table 1 Parameters used in PDEs for fuel oxidation model

Term	Description	Expression	Units
D	Diffusion coefficient of oxygen in UO_2 matrix	$\left(2.5\times10^{-4}\right)\exp\left(-\frac{16400}{T}\right)$	$m^2\ s^{-1}$
Q^*	Heat of transport of oxygen in UO_2 matrix	$-3.5\times10^{34}\exp\left(-17\left(4+2x\right)\right)$	$J\ mol^{-1}$
R	Ideal gas constant	8.314	$J\ mol^{-1}\ K^{-1}$
σ_{fuel}	Surface-area-to-volume ratio of UO_2	$\left\{\begin{array}{c}908, T<1473K\\ 908\times\left(0.0025T-3.6825\right), 1473K\le T\le1873K\\ 0, T>1873K\end{array}\right\}$	m^{-1}
R_{fuel}^{react}	Oxidation/reduction kinetics term	$\left\{\begin{array}{c}\alpha\sqrt{\left(1-q\right)p_t}\left(x_e-x\right), x\le x_e\\ \alpha\sqrt{qp_t}\left(x_e-x\right), x>x_e\end{array}\right\}$	$m\ s^{-1}$
α	Oxidation surface exchange coefficient	$0.365\exp\left(-\frac{23500}{T}\right)$	$m\ s^{-1}$
p_t	Total system pressure	100	atm
c_u	Molar density of UO_2	$4.1\times10^4\rho_{fix}\left(1-P\right)$	$mol\ U\ m^{-3}$
ρ_{fix}	Density normalized with respect to ρ_{273}	$\left\{\begin{array}{c}\left(0.99734+9.802\times10^{-5}T-2.705\times10^{-10}T^2+4.391\times10^{-13}T^3\right)^{-3}, 273K\le T\le923K\\ \left(0.99672+1.179\times10^{-5}T-2.429\times10^{-9}T^2+1.219\times10^{-12}T^3\right)^{-3}, T>923K\end{array}\right\}$	-
P	Fuel porosity	$0.0282846715\left(1-F\right)$	-
F	Burnup-dependent change in fuel porosity	$0.6-\exp\left\{-0.506-8.67\times10^{-10}T^3\left[1-\exp\left\{-2.87\times10^{-2}\beta\right\}\right]\right\}$	-
β	Fuel burnup	0 to 235	$MWh\ kg\ U^{-1}$
C_p	Heat capacity of UO_2	$52.1743+45.8056x+\left(87.951\times10^{-3}-7.3461\times10^{-2}x\right)T$ $+\left(1-x\right)\left\{-84.2411\times10^{-6}T^2+31.542\times10^{-9}T^3-2.6334\times10^{-12}T^4\right\}$ $-\left(713910+295090x\right)T^{-2}$	$kJ\ mol^{-1}\ K^{-1}$
k	Corrected thermal conductivity of UO_2	$\kappa_{1d}\kappa_{1p}\kappa_{2p}\kappa_{4r}k_{2+x}$	$kW\ m^{-1}\ K^{-1}$
κ_{1d}	Factor for dissolved fission products	$\left(\frac{1.09}{\beta^{3.265}}+\frac{0.0643}{\sqrt{\beta}}\sqrt{T}\right)\arctan\left(\frac{1}{1.09/\beta^{3.265}+\left(0.0643/\sqrt{\beta}\right)\sqrt{T}}\right)$	-
κ_{1p}	Factor for precipitated fission products	$1+\frac{0.019\beta}{\left(3-0.019\beta\right)\left(1+\exp\left\{-\left(T-1200\right)/100\right\}\right)}$	-
κ_{2p}	Factor for porosity effects	$\left(1-\left(2.6-0.5\times10^{-3}T\right)P\right)$	-
κ_{4r}	Factor for radiation effects	$1-\frac{0.2}{1+\exp\left\{\left(T-900\right)/80\right\}}$	-
k_{2+x}	Uncorrected thermal conductivity of UO_2	$k_{ph}+k_e$	$kW\ m^{-1}\ K^{-1}$
k_{ph}	Phonon contribution to thermal conductivity	$\frac{1}{A+BT}$	$kW\ m^{-1}\ K^{-1}$
A	Phonon-phonon interaction term	$14-10.763x^{0.5}-2381.4x+12819.86x^{1.5}$	$K\ m\ kW^{-1}$
B	Phonon-polaron interaction term	$\left\{\begin{array}{c}0.2218+0.2562\sqrt{x}-0.64x-3.6764\left(\sqrt{x}\right)^3, x<0.155\\ 0, x\ge0.155\end{array}\right\}$	$m\ kW^{-1}$
k_e	Polaron contribution to thermal conductivity	$\left(0.87+2.5\times10^{-5}T\right)^{-1}\frac{2.024\times10^8}{T^{5/2}}\exp\left(-16350/T\right)$	$kW\ m^{-1}\ K^{-1}$
P_{lin}	Linear power rating	20 to 65	$kW\ m^{-1}$
a_p	Pellet radius	6.075 to 7.150	mm
κ	Neutron diffusion length	110	m^{-1}

Equation 3 is solved assuming no oxidation at initialization, an axial symmetry condition at the centreline, and no reaction ($x = x_e$) at the fuel surface. Equation 5 is solved assuming an initial temperature equal to the fuel surface temperature, which is evaluated according to the methodology of Lewis et. al.[4,6], and insular boundaries at the axial edges and centreline of the element.

3.2 Development of Empirical Correlations

The effects of gas-phase transport in the radial fuel cracks and axial solid-state diffusion of oxygen are captured using correlations for the hydrogen mole fraction q and the axial relaxation length ξ, respectively. Based on a sensitivity analysis of the stoichiometry deviation as predicted by the mechanistic model with respect to different fuel conditions, the correlations were determined as functions of the parameters in Table 2.

Table 2 Variable parameters used to develop empirical correlations

Parameter	Range (Units)	Units
Linear power rating	$20 \rightarrow 65$	kW m^{-1}
Number of defects	$1 \rightarrow 4$	-
Defect size (axial length)	$0.1 \rightarrow 80$	mm
Distance between defects	$0 \rightarrow 450$	mm
Post-Defect Residence Time (PDRT)	$1 \rightarrow 760$	d

The time-dependence of q is implicitly captured by assuming a constant average value for the full element PDRT. A representative case determining the average value of q at the fuel centreline directly beneath a defect site, based on the time-dependent profile from a mechanistic model simulation of an element operating at 40 kW m^{-1} for 380 d with a single 5-mm defect at the element midplane, is shown in Figure 3. The centreline average values of q for the full space of element linear powers and defect sizes shown in Table 2 were reproduced using orthogonal Legendre polynomials (see Appendix), which can be defined recursively to produce the required precision.

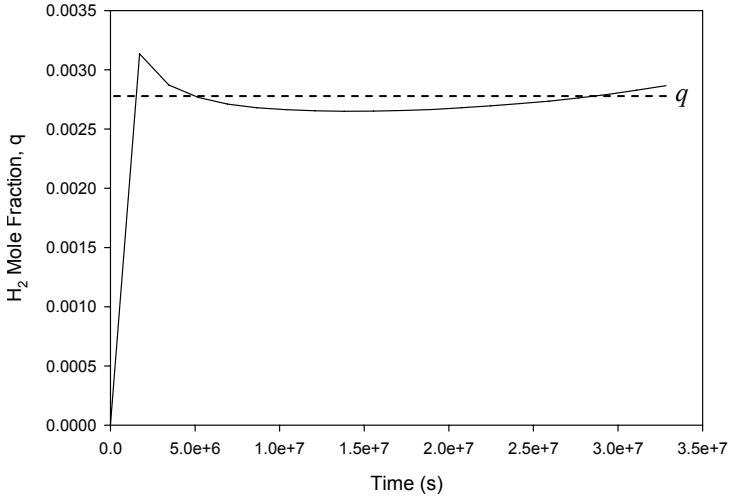

Figure 3 Centreline q beneath the site of a 5-mm defect for a fuel element operating at 40 kW m^{-1} for a PDRT of 380 d with the average value indicated by the dashed line.

At the defect site at the fuel surface, the hydrogen mole fraction is effectively zero, as any excess hydrogen released by the fuel cracks would axially diffuse away from the defect site or be swept away by the coolant stream to which the defect site is exposed. The radial

profile of the hydrogen mole fraction between the fuel centreline and fuel surface is determined by temperature-dependent gas-phase diffusion and restructuring of the fuel. Between the temperatures of 1473 and 1873 K, plastic healing of the fuel cracks occurs, suppressing diffusion of hydrogen in this region. Thus, the radial profile differs between the elastic region (T<1473 K), and the region of plastic healing (1473 K < T < 1873 K)and so is approximated using a combination of two linear profiles as shown in Figure 4. In the fully plastic region (T > 1873 K), no gas is present and so there is no hydrogen mole fraction and no reaction.

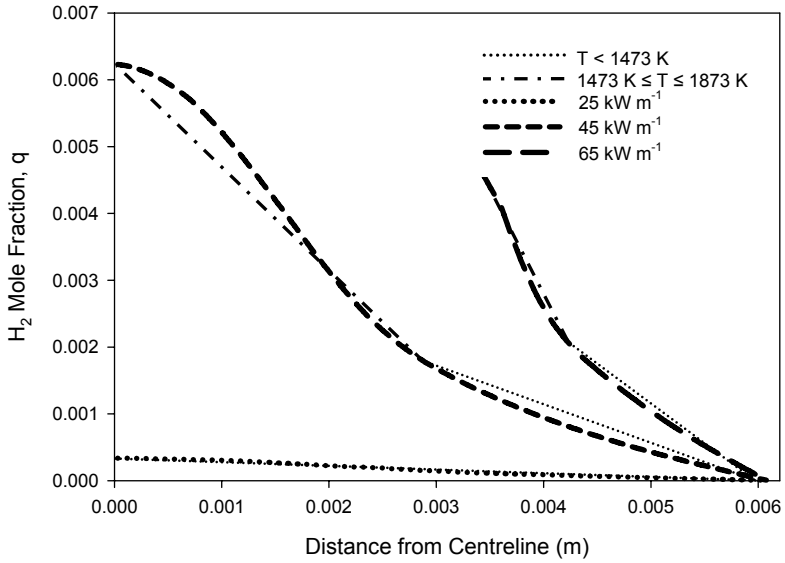

Figure 4 Radial profiles of H_2 mole fraction q under a 1-mm defect for elements operating at three different linear power ratings as predicted by the mechanistic model, with linear approximations to the profiles as used in the simplified model.

Below 1873 K, the H_2 mole fraction at the fuel centreline (q_{cent}) is determined by the Legendre polynomials for the given power rating and defect size, and the surface value (q_{surf}) is always a near-zero constant. However, values of q at T = 1473 K and T = 1873 K are required in order to produce the correct profiles for higher-power cases where such temperatures are reached. Using a typical defect size of 1 mm, two additional correlations were developed (see Appendix). The first determines $q_{T=1873}$ for high-power cases, and the second relates $q_{T=1473}$ to the maximum q (equal to q_{cent} or $q_{T=1873}$ depending on the power, as seen in Figure 4). By coupling the radial profile to temperature, a more realistic time dependence is incorporated into the simplified model.

Given the predicted radial profile for the H_2 mole fraction q, Equations 3 and 5 can be used to predict the radial profile of stoichiometry deviation x under the defect site, where the equilibrium stoichiometry deviation x_e and the reaction rate R_{fuel}^{react} are both functions of q as seen in Figure 1 and Table 1, respectively. To predict the axial oxygen profile away from the defect site using Equation 4, an additional correlation is needed for the axial relaxation length ξ. Assuming that ξ is constant with respect to axial separation from the defect site z_{sep}, Equation 4 can be solved to give:

$$\xi = -\frac{1}{z_{sep}} \ln\left(\frac{x(z_{sep})}{x_{def}}\right) \qquad \textbf{Equation 6}$$

Running the mechanistic model for the full range of element linear power ratings and distances between defects given in Table 2, a full space of values for ξ was produced for axial profiles between both a defect and the axial edge of the element, and for profiles between two different defects. The sets of values for each of these cases were reproduced using two different correlations (see Appendix).

By introducing the correlations for H_2 mole fraction at the fuel centreline, the radial profile for H_2 mole fraction, and the axial relaxation length to Equations 3, 4, and 5, the fuel oxidation state and temperature can be predicted for the two-dimensional fuel geometry.

4 Results and Discussion

4.1 Model Validation for Normal Operating Conditions

The simplified fuel oxidation model outlined in Section 3 was implemented in COMSOL Multiphysics™ and used to predict the oxidation and temperature profiles of 10 commercial defective fuel elements, which were measured for their oxygen-to-metal (O/M) ratios. In particular, the results were compared to the predictions of the mechanistic model and to experimental data provided by Atomic Energy of Canada Limited (AECL) at the Chalk River Laboratories (CRL)[7]. At the CRL, the O/M ratio was measured for each of the defective elements using a coulometric titration (CT) technique. For a representative case, a comparison of results is shown in Figure 5.

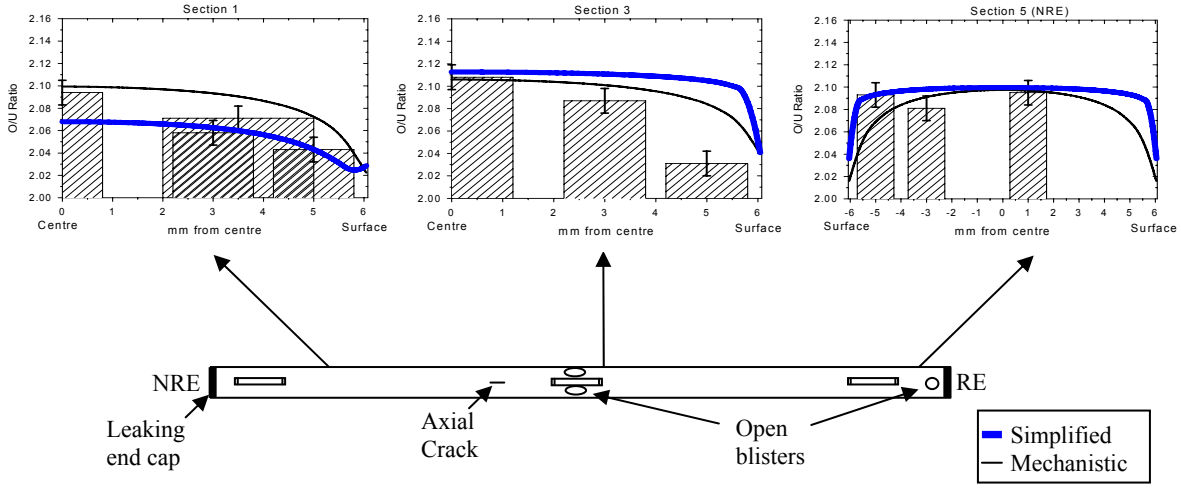

Figure 5 Representative comparison of model predictions to CRL measurements of O/U ratio.

There were no *in-situ* measurements of the fuel centreline temperature, and so only the temperature values from the simplified and mechanistic models can be compared. In general, the predicted results of the O/M ratio compare well with the mechanistic model predictions, and with the measured CT data. Also, the predictions of the centreline temperature typically vary by less than ~100 K (up to 175 K), suggesting reasonable

™ COMSOL Multiphysics is a trademark of Comsol AB.

agreement between the two models. Fuel centreline melting is never predicted for these ten commercial defective cases.

In some cases, the simplified model shows some underprediction of the fuel stoichiometry deviation and fuel centreline temperature, highlighting some limitations of the model. Most significantly, by reducing the oxygen transport equation to one dimension, conservation of oxygen mass is no longer maintained in the non-defective regions of the fuel. For specific cases where defects are close to the element endcaps, axial diffusion should increase the stoichiometry deviation under the defect site and between the defect site and the endcap, an effect which is not captured if conservation of mass is not maintained. Also, for cases where the element linear power rating changes over time, the change in axial relaxation length cannot account for the oxygen previously present in the non-defective regions without a condition requiring 2-dimensional mass conservation. Simulations have been performed demonstrating that using a two-dimensional oxygen transport equation re-introduces conservation of mass and eliminates the underprediction of fuel hyperstoichometry.[6] However, the use of a two-dimensional equation would increase the complexity of the model, which contravenes the need for a simplified treatment for ease of implementation and model robustness.

4.2 Application to Transient Analysis

It is specifically important to know if and when the fuel undergoes centreline melting. It has been demonstrated in this work that, for typical normal operating conditions (NOC), fuel melting is not expected. However, a remaining question is whether centreline melting could occur in a previously defective element (where the fuel has already been oxidized) during an accident scenario, such as a Loss-of-Coolant Accident (LOCA).

During a LOCA, as a result of coolant voiding and the positive void coefficient, there is a sharp increase in the power rating of a fuel bundle, and a concurrent temperature increase in the fuel sheath and fuel itself for a short duration. The increased fuel temperatures are depicted in Figure 6 based on a BEAU (Best Estimate And Uncertainty) methodology[6].

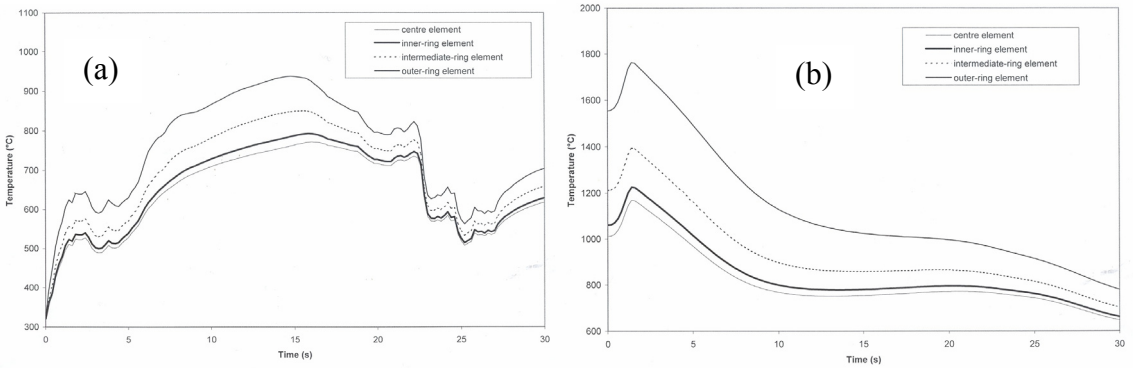

Figure 6 Transients for typical BEAU conditions for (a) fuel sheath temperature and (b) fuel centerline temperature. Taken from [6].

The mechanistic and simplified models were used to simulate a fuel element undergoing a LOCA for 3 s under the conditions for normalized power (assuming an initial linear power rating of 63 kW m^{-1}) and sheath temperature given by the BEAU analysis. Three possible scenarios were considered assuming (i) an intact element, (ii) a defective element with no fuel-to-sheath gap, (iii) a defective element with a fuel-to-sheath gap

with an estimated 10-μm thickness. A comparison of predicted fuel centreline temperatures for these three scenarios, and for the mechanistic and simplified models, is shown in Figure 7(a).

The temperatures reached during the LOCA are below the incipient melting temperature for UO_2. However, it is also of interest to determine whether the fuel stoichiometry changes during the power pulse. Simulations were therefore performed with both the mechanistic and simplified models where the radial profile of the fuel stoichiometry deviation was examined under the defect site at various times (see Figure 7(b)) for the given fuel centerline temperature history.

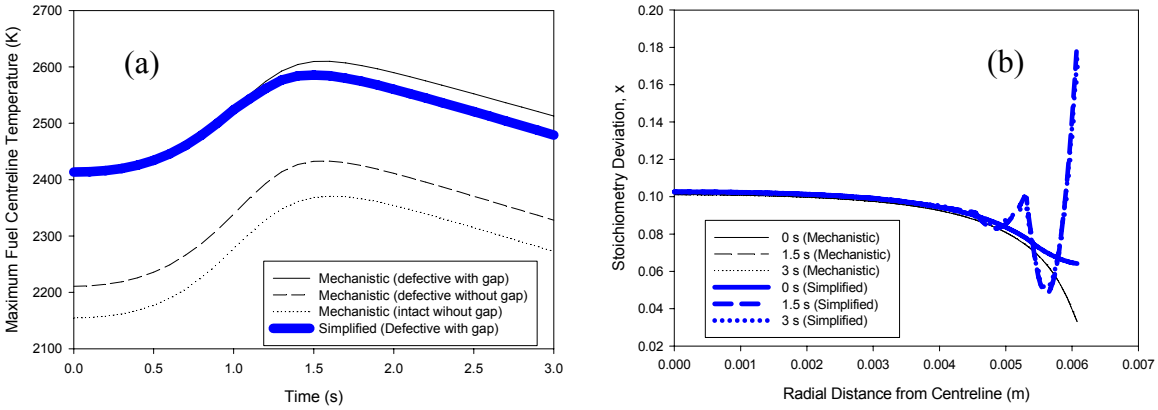

Figure 7 Predicted history of (a) fuel centreline temperature, and (b) radial stoichiometry deviation profile under the defect site, for the power pulse using the mechanistic model for intact and defective fuel simulations and the mechanistic and simplified models for defective fuel (with a gap).

As expected, the oxidation state remains unchanged, which indicates that there is insufficient time during the power pulse for the fuel oxidation reaction kinetics and solid-state diffusion of interstitial oxygen to occur. For the simplified model, there is some fluctuation in the stoichiometry deviation curve at and near the fuel surface position due to a numerical artifact of the surface boundary condition, where x is set equal to x_e in contrast to the use of a zero-flux condition for the mechanistic model. However, this slight effect does not affect the radial profile away from the fuel surface.

In fact, with any possible metal-water reaction at high temperature conditions, an increased concentration of hydrogen could potentially lower the oxygen potential, thus decreasing the likelihood of fuel oxidation. Moreover, with the presence of hydrogen, the fuel reduction kinetics are considerably faster than the fuel oxidation kinetics as observed in high-temperature annealing experiments conducted at the University of California (UCL)-Berkeley[8]. Thus, one would not expect further fuel oxidation during the transient.

5 Conclusions and Recommendations

A robust simplified model has been developed for predicting the oxidation behaviour of typical defective CANDU fuel elements. The current model is in agreement with published experimental data for fuel stoichiometry deviation, and with the mechanistic model for fuel stoichiometry deviation and temperature. The simplified model has been tested for both normal and typical transient circumstances. As demonstrated, there is no

centreline melting and in particular, no change in the oxidation state of the fuel during a power pulse starting from a high power rating. The simplified model could potentially be incorporated into fuel performance codes[9,10] in order to include the effects of fuel oxidation on fuel performance behaviour with possible failure of the sheath during normal and reactor accident conditions.

References

1. B.J. Lewis, R.D. MacDonald, N.V. Ivanoff, and F.C. Iglesias, "Fuel Performance and Fission Product Release Studies for Defected Fuel Elements," Nucl. Technol. 103 (1993) 220.
2. A. Viktorov and M. Couture, "Regulatory Activities in the Area of Fuel Safety and Performance," Canadian Nuclear Safety Commission, Presented at the 9th Int. Conf. On CANDU Fuel, Belleville, ON, 17-21 September 2005.
3. J.C. Ramirez, M. Stan, P. Cristea, "Simulations of heat and oxygen diffusion in UO_2 nuclear fuel rods," J. Nucl. Mater. 359 (2006) 174-184.
4. J. Higgs, "Modelling Oxidation Behaviour in Operating Defective Nuclear Reactor Fuel Elements," PhD. Thesis, Royal Military College of Canada, January 2006.
5. J.D. Higgs, B.J. Lewis, W.T. Thompson and Z. He, "A conceptual model for the fuel oxidation of defective fuel," J. Nucl. Mater. 366 (2007) 99-128.
6. K. Shaheen, "A Simplified Oxidation Model for Defective Nuclear Fuel," MASc. Thesis, Royal Military College of Canada, December 2007.
7. R.A. Verrall, Z. He, J.F. Mouris, "Characterization of fuel oxidation in rods with clad-holes," J. Nucl. Mater. 344 (2005) 240-245.
8. J. Abrefah, A. de Aguiar Braid, W. Wang, Y. Khalil and D.R. Olander, "High Temperature Oxidation of UO_2 in Steam-Hydrogen Mixtures," J. Nucl. Mater. 208 (1994) 220-245.
9. G.G. Chassie, K-S. Sim, B. Wong, G. Papayiannis, "ELESTRES Code Upgrades," AECL, 9th International CNS Conference on CANDU Fuel, 2005.
10. A.F. Williams, "The ELOCA Fuel Modelling Code: Past, Present and Future," 9th International CNS Conference on CANDU Fuel, 2005.

Appendix: Correlation Expressions for q and ξ

In the current treatment, the H_2 mole fraction at the fuel centreline q_{cent} is expressed as a function of the normalized linear power of the defective element:

$$q_{cent}(P_{lin}) = a_0P_0 + a_1P_1 + a_2P_2 + a_3P_3 + a_4P_4 + a_5P_5 \quad \textbf{Equation 7}$$

where the terms P_n are Legendre polynomials defined by:

$$(n+1)P_{n+1} = (2n+1)\cdot P_{norm}\cdot P_n - nP_{n-1} \quad n = 1,2,3,.. \quad \textbf{Equation 8}$$

where the first two polynomials are $P_0(P_{norm}) = 1$ and $P_1(P_{norm}) = P_{norm}$. P_{norm} is the power rating normalized with respect to a maximum of 45 kW m^{-1}. Accordingly, the polynomial coefficients in Equation 8 are given in Table 3 below as a further function of defect size.

Table 3 Legendre polynomial coefficients

N	0	1	2	3	4	5
Defect size (mm)	**Legendre polynomial coefficient, a_n**					
0.1	-3.3842	7.7475	-7.3670	4.2106	-1.4253	0.2256
1	-2.8710	6.5984	-6.3248	3.6608	-1.2616	0.2050
5	-1.6649	3.8337	-3.6891	2.1531	-0.7530	0.1268
10	0.9579	-2.1695	2.0267	-1.1178	0.3605	-0.0512
20	0.1928	-0.4351	-0.4083	-0.2220	0.0706	-0.0081
50	-0.6036	1.3885	-1.3295	0.7735	-0.2687	0.0462
80	-0.3487	0.8033	-0.7689	0.4491	-0.1562	0.0275

For power ratings above 45 kW m^{-1}, the centreline temperatue exceeds 1873 K and so there is no hydrogen at the fuel centreline. A separate correlation is used to determine $q_{T=1873}$ for power ratings above 45 kW m^{-1}, to a maximum of 65 kW m^{-1}:

$$q_{T=1873} = 0.007406305 + 0.0038311007 \cdot \exp\left(-0.5\cdot\left(\frac{\ln(P_{lin}/54.524176)}{0.082161078}\right)^2\right) \quad \textbf{Equation 9}$$

To determine the radial profile of q, an additional correlation predicts the ratio of $q_{T=1473}$ to the maximum value of q_{max} (q_{cent} *or* $q_{T=1873}$, depending on the power rating). The correlations in both Equation 9 and Equation 10 are developed using TableCurve2D™:

$$\frac{q_{T=1473}}{q_{\max}} = 82.232326 - 5.8829754\cdot P_{lin} + 0.15665173\cdot P_{lin}^{\,2} - 0.001840115\cdot P_{lin}^{\,3} + 0.0000080548\cdot P_{lin}^{\,4} \quad \textbf{Equation 10}$$

The axial relaxation length ξ (m^{-1}) is expressed using two correlations produced using TableCurve3D™, depending on whether the axial transport is being estimated between two defects or between a defect and the axial edge of an element. For the former case:

$$\ln(\xi) = a + bP_{lin} + cP_{lin}\ln(P_{lin}) + dP_{lin}^{\,1.5} + eP_{lin}^{\,2} + \frac{fP_{lin}}{\ln(P_{lin})} + \frac{g}{dist^{\,1.5}} \quad \textbf{Equation 11}$$

where a= -13161.114, b= -3613.2804, c= 422.94119, d= -19.387802, e= -0.23369769, f= 9274.4627, g= -0.01697377, and *dist* is the distance between defects. For the latter case:

$$\xi = \frac{a + b\ln(P_{lin}) + c(\ln(P_{lin}))^2 + d(\ln(P_{lin}))^3 + e\ln(dist) + f(\ln(dist))^2}{1 + g\ln(P_{lin}) + h(\ln(P_{lin}))^2 + i\ln(dist) + j(\ln(dist))^2} \quad \textbf{Equation 12}$$

where a= 84.265577, b= -63.893832, c= 16.142395, d= -1.3561087, e= 0.10732054, f= 0.01932394, g= -0.56834412, h= 0.081072625, i= 0.0048176509, j= 0.002439633, and *dist* is the distance between the defect and the axial edge of the element.

™ TableCurve2D and TableCurve3D are trademarks of SPSS, Inc